Scalar mixing in bubbly flows: Experimental investigation and diffusivity modelling

E. Alméras [a,b], C. Plais [a], F. Euzenat [a], F. Risso [b], V. Roig [b], F. Augier [a,*]

[a] IFP Energies nouvelles, Rond-point de l'échangeur de Solaize, BP 3, 69360 Solaize, France
[b] IMFT, Université de Toulouse and CNRS, Allée C. Soula, 31400 Toulouse, France

HIGHLIGHTS

- Diffusion coefficient of a scalar in bubbly flows.
- Mixing by Bubble-Induced Turbulence.
- Effective diffusivity implemented in a two-fluid model.
- Validation by comparison between experiments and CFD results.

ABSTRACT

Transport properties of scalars, as concentrations of a solute or temperature, are important for scale-up and design of operation units. An appropriate description of convective and diffusive mechanisms is required to predict local concentrations in complex geometries. In the case of gas–liquid bubbly flows, which are present in many chemical- or bio-reactors, effective diffusivity of scalars results from three contributions: molecular diffusion, Shear-Induced Turbulence (S.I.T.), i.e. turbulence induced by gradients of velocity in the continuous phase, and Bubble-Induced Turbulence (B.I.T.), i.e. turbulence generated by interactions of bubble wakes. In a previous work (Alméras et al., 2014, 2015), the diffusion resulting from B.I.T. has been characterized. Based on experiments performed in a homogeneous bubble column, it has been shown that the transport can be modelled by an effective diffusion and a physical modelling has been proposed to predict the diffusion induced by B.I.T. when other contributions are negligible.

In the present work, we investigate the transport of a passive scalar in a complex bubbly flow at moderate gas volume fraction ($\alpha_g \leq 3\%$), involving a large-scale flow recirculation responsible for the development of Shear-Induced Turbulence. Experimental mixing times measured by image processing under various operating conditions have been compared to numerical simulations of scalar transport. Simulations have been performed by means of an Eulerian RANS CFD model wherein the diffusion generated by B.I.T. modelled by Alméras et al. (2015) is implemented in addition to the diffusion resulting from the S.I.T.

Results show that the diffusion caused by B.I.T. plays a major role in the mixing of scalars in the investigated flows. Neglecting this contribution leads to an important overestimation of the mixing time unless assigning arbitrary low values to the turbulent Schmidt number Sc_t (< 0.3) adapted a posteriori to the simulated cases. On the other hand, considering the scalar diffusivity by B.I.T leads to a good agreement between experiments and CFD simulations, with keeping the Schmidt number in the usual range adopted for mixing in S.I.T. [0.7–1]. The model is generic enough to reproduce the scalar transport for various gas injections, without any further user adaptation.

Keywords:
Bubbly flows
Bubble column
Scalar diffusivity
Mixing
CFD
Experiment

1. Introduction

Bubbly flows are very common in many industrial fields such as biology, chemistry, refining, and water treatment. They can be implemented in various contacting apparatus as aerated stirred reactors, bubble columns, air-lift columns (Laurent and Charpentier,

* Corresponding author.
E-mail address: frederic.augier@ifpen.fr (F. Augier).

http://dx.doi.org/10.1016/j.ces.2015.10.010

1974). Resulting hydrodynamics is generally complex due to the presence of different sources of agitation as macro-scale recirculation, buoyancy-driven instabilities, turbulence and relative motion between phases. Depending on the technology and the geometry of contactors, overall hydrodynamics responsible for concentration transport skips from quasi-plug flow to well stirred flow (Deckwer,1992). The prediction of global hydrodynamics is a major issue for process design as it strongly impacts performances of considered gas–liquid contacting units.

In this goal, as an alternative to expensive experimental studies, Computational Fluid Dynamics (CFD) is a very powerful tool for prediction of global and local hydrodynamics. It has been applied for decades to gas–liquid flow characterization (Delnoij et al., 1997; Rafique et al., 2004) and nowadays, different types of models exist to simulate bubbly flows. For example, interface reconstruction models such as Volume of Fluid models (VOF) allow to predict the bubble size and shape (Li et al., 2000; Dai et al., 2004) while Lagrangian models can calculate individual bubble trajectories (Lau et al., 2014). But these two families of models are still unable to predict dense bubbly flows at large industrial scales because the calculation of each bubble position and/or shape is too-much CPU-time consuming and that bubbles interactions are difficult to reproduce. Large geometries involving bubbly flows are often simulated by using the so-called two-fluid models (Jakobsen et al., 2005). The formalism of two-fluid models is based on phase-volume and time averaging (Zhang and Prosperetti, 1994). As a consequence, mean phase velocity and fraction fields are solved. The two phases are considered as two interpenetrating continuous phases and mass and momentum balances are solved for both fluids including their transfers at the interfaces. Turbulence can be described by different approaches, such as mixing-length models (Lance et al., 1996), two-equation models like the popular $k-\varepsilon$ one (Laborde-Boudet et al., 2009), or Large Eddy Simulation (LES) models (Dhotre et al., 2009). In the last case, velocity fluctuations associated with large eddies are resolved while small scales are determined by appropriate Sub-Grid-Scale models. Literature abounds of works dealing with benefits and limits of every kind of turbulence models (Jakobsen et al., 2005).

When transport of chemical species is required in CFD simulations, an important issue concerns the contribution of velocity fluctuations that are not explicitly solved. The transport equation of the concentration describes only the contribution of the average velocity while the diffusivity induced by velocity fluctuations is taken into account through closure laws involving turbulence characteristics. Concerning single-phase flows, a simple solution consists in using a turbulent Schmidt number (Sc_t) to estimate the contribution of turbulence to the global diffusivity of passive scalars (Combest et al., 2011):

$$D_t = \frac{\nu_t}{Sc_t} \tag{1}$$

The Sc_t approach is considered as classical and well validated. Different values of Sc_t in the range [0.7–1] may be preconised following the type of flow (Combest et al., 2011). In case of turbulent dispersed flows, scalar diffusion can result from turbulence induced both by the velocity gradients and by the agitation generated by the bubbles. One first possibility is to include the effect of bubbles within a global turbulent diffusivity. As bubbles increase the local fluid agitation, the apparent Schmidt number may be lower than the value classically used for single-phase flows. Radl and Khinast (2010) report values between [0.4 and 0.7] depending on the turbulence model. This pragmatic approach can lead to satisfying results even if it is not based on a strong theoretical asset. It is however only appropriate when Shear-Induced Turbulence is largely dominant compared to B.I.T. Eq. (1) obviously leads to a low diffusivity when turbulent viscosity tends towards zero although under such conditions Bubble-Induced Turbulence still disperses passive scalars. Sato et al. (1981) propose an alternative approach by directly including the contribution of bubble wakes in the turbulent viscosity ν_t. This approach is however not able to deal with the decrease of ν_t caused by the presence of bubbles that is observed in some cases (Serizawa et al., 1992), and is therefore more suitable for flows governed by wall-induced turbulence. More recently, Ayed et al. (2007) also introduced a supplementary diffusivity due to bubble motions, which leads to an additional scalar diffusivity proportional to $\alpha_g d U_R$, in agreement with Sato et al. (1981). Politano et al. (2003) proposed a contribution of B.I.T. to the Reynolds stress tensor that may affect the turbulent viscosity and diffusivity in the presence of velocity gradients. This contribution tends to zero in the case of homogeneous flows with no gradient of gas fraction and is thus not suitable for the present study. Following Troshko and Hassan (2001), Rzehak and Krepper (2013) added source terms in k and ε transport equations to model the effect of the drag on turbulence. The use of the latter models to transport scalars implicitly involves that Shear and Bubble Induced Turbulence contribute similarly to the turbulent diffusivity through the turbulent viscosity, which is far to be established.

Adding a specific diffusivity to account for the contribution of the bubbles to the mixing seems a more relevant approach referring to the experimental work of Alméras et al. (2014, 2015), as this allows to dissociate the effect of both types of turbulence on the diffusivity. This work has shown that the mixing induced by bubbles is well described by a regular diffusion process, the effective diffusion coefficients of which have been measured in vertical and horizontal directions for gas holdup from 1% to 13%. Following the Taylor's, 1921 approach, Alméras et al. propose to write the diffusivity coefficient $D_{i,i}$ as the product of the variance of the velocity fluctuations $u_i'^2$ by a diffusion timescale T_m ($D_{i,i} \propto u_i'^2 T_m$). As described by Lance and Bataille (1991) or Riboux et al. (2010), the variance of the velocity fluctuations currently evolves as $u_i'^2 = \gamma_i^2 U_R^2 \alpha_g$. Concerning the diffusion timescale, two regimes of diffusion have been identified depending on the holdup. At low holdup, the diffusion timescale is evaluated as $T_m = \Lambda / u_i'$ (Corrsin, 1963), where Λ is the Eulerian integral length scale which does not depend on the holdup (Riboux et al., 2010). Consequently, at low holdup, the diffusion coefficient evolves like $\alpha_g^{0.5}$ (Alméras et al., 2015). At large holdup, the diffusion timescale is limited by the average time interval between two bubbles passages, which is proportional to $\frac{d}{(\alpha_g U_R)}$. In this case, the diffusion coefficient is proportional to $U_r d$ and independent of α. It is important to notice that due to the anisotropy of the velocity fluctuations, the mixing induced by bubbles is anisotropic whatever the diffusion regime. The diffusion coefficient in the vertical direction is twice or even larger than that in the horizontal direction. Moreover, the transition between the two diffusion regimes occurs for a lower holdup in the horizontal direction than in the vertical one.

Based on the analysis of Alméras et al. (2015), the following model for the diffusion coefficients which accounts for the mixing by the B.I.T. is proposed

$$D_{i,i} = \begin{cases} D_{i0} \alpha_g^{0.5} & \text{if} \quad \alpha_g \le \alpha_{gc,i} \\ \beta \gamma_i^2 U_R d & \text{if} \quad \alpha_g > \alpha_{gc,i} \end{cases} \tag{2}$$

With the parameters reported in Table 1. Note that $D_{i0} = a_i U_R \Lambda$, where the prefactors a_i have been adjusted so that the diffusion coefficients in the vertical direction ($D_{x,x}$) and in the horizontal direction ($D_{y,y}$) are continuous at $\alpha_{gc,x}$ and $\alpha_{gc,y}$, respectively. It is also important to notice that this model differs from those of Sato et al. (1981) and Ayed et al. (2007) which introduce diffusion coefficients that are proportional to α_g. To sum up, there are

various possibilities to account for the effect of bubbles on scalar diffusivity. A simple adjustment of the turbulent Schmidt number is attractive for engineers but needs to be validated for each kind of application as it may hide more complex phenomena. On the other hand, recent developments concerning diffusion by B.I.T. such as the model described by Eq. (2), are promising but restricted to truly homogeneous bubbly flows. Note that here the word homogeneous is used in its most restrictive mathematical sense and means that there is no gradient of any statistical quantity such as mean velocity or phase fraction. It should not be confused with the common practical classification of bubble columns (Deen et al., 2010; Kantarci et al., 2005) in which flows with moderate gradients are still considered as homogeneous, and heterogeneous designates churn flows. We now need to assess whether the diffusion by S.I.T. and by B.I.T can be added to address practical situations where both types of turbulence are present.

In the present work, it is proposed to study bubbly flows under moderate non-homogeneous conditions with the aim to test the relevance of the model of Alméras et al. (2015) for practical situations. A 37 L air/water bubble column is used with a gas injection that generates a flow recirculation. Low gas flow rates ($V_{sg} < 1$ cm/s) are investigated in order to produce flows that are relatively easy to simulate with two-fluid models and where turbulence and bubble wakes may generate diffusivities of similar magnitudes. This configuration is also relevant for some bubbly reactors that are operated at low gas velocities.

First, mixing time experiments are performed by means of a colorimetric method. An in-house image processing is used to estimate mixing times. The method has been previously developed to measure mixing times in aerated stirred bioreactors (Gabelle et al., 2011). In a second step, hydrodynamics of investigated flows is modelled using a two-fluid CFD code. Once hydrodynamics is validated, simulations of tracer injections are performed in order to compare simulated overall mixing times to measured ones.

Table 1
Parameters of the diffusivity model of Alméras (2014) where x is the vertical direction, y the horizontal one.

$\alpha_{gc,x}$	$\alpha_{gc,y}$	D_{x0} (m^2/s)	D_{y0} (m^2/s)	γ_x	γ_y	β
0.041	0.027	0.0045	0.0029	0.18	0.13	25

Scalar mixing is simulated for different values of Sc_t, and with or without adding the diffusivity model of Alméras et al. (2015). Conclusions are drawn from comparisons between experiments and CFD simulations and recommendations are proposed concerning the modelling of scalar transport in bubbly flows.

2. Experimental setup and measurement method

A schematic representation of the experimental setup is shown in Fig. 1. Experiments are carried out in a 300-mm diameter cylindrical glass column. The height of water is $H = 0.53$ m for each experiment. Concerning air injection, three types of distributor plates have been used. The first distributor (#1) is a plane plate of diameter 25 cm, drilled of 35 holes equally spaced. The holes have a diameter of 1 mm and follow a triangular step of 4 cm. The second distributor (#2) is a modification of the first one, 31 holes have been clogged up using tape in order to allow air only through a central ring of 6 holes. The third one (#3) involves only 15 holes, all being located on the same half-section of the whole distributor. Only the first distributor has been used for comparison with CFD. Fig. 1 presents the complete distribution device. After 10 min of flow stabilisation, 10 mL of a dye tracer (Purple Drimarene R 2RL Clariant®) are injected by an injection device located at the centre of the column and at 9 cm above the perforated bottom plate. The injection device is equipped with a splash plate that maintains the dye close to the injection point during the injection. The time of injection is approximately 2 s. Immediately after each tracer injection, water is sent to rinse the injection pipe. This also shortens the effective time of injection. Fig. 2 illustrates the injection of dye and its mixing in the tank for the first and second gas distributors at different times after injection.

The global gas volume fraction α_g is measured by the elevation of the liquid level at the top of the column. The accuracy of the measurement is estimated to be $\pm 0.2\%$ of the absolute gas holdup. The mean bubble size is measured by photography and semi-manual image treatment, with an error of ± 0.5 mm. A SLR camera equipped with a Nikkon 60 mm f2.8 lens is used at 1600 ISO, with a shutter speed of 1/800 s. Led white panels are used to lighten the flow. Images are processed by Image J free software. Small and large diameters of deformed bubbles are manually measured, and used to estimate their volume and surface

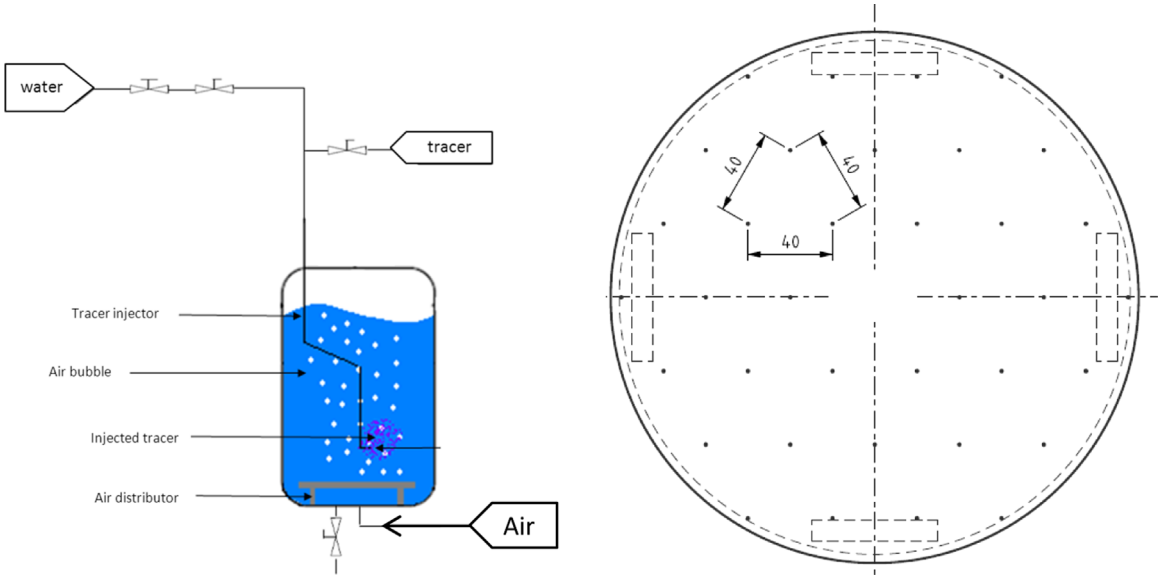

Fig. 1. Schematic of the experimental setup: 300 mm diameter bubble column, air distributor and tracer injection. To the left: side view. To the right: top view of the air distributor.

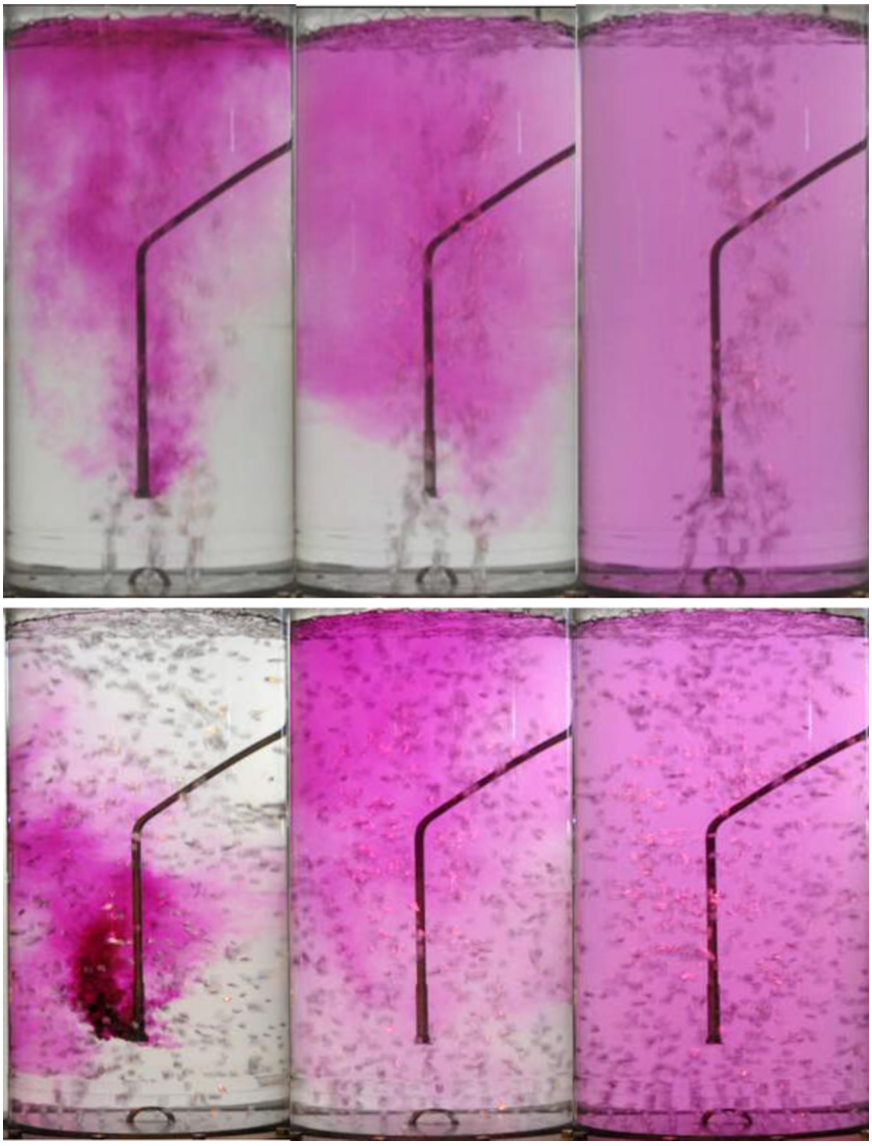

Fig. 2. Dye injection and mixing at different times. First row: distributor 1. Second row: distributor 2. From left to right: Q_g=0.5 m^3/h. t=2 s, 6 s and ∞.

assuming oblate shapes. The mean Sauter diameter is estimated from the measurement of approximately 200–300 bubbles. The camera is also used to record the injection of the dye and the mixing inside the tank. Mixing times are determined thanks to an in-house image processing software. Pictures are divided into 6 windows of 1 cm^2 and the mean grey level inside each window (maximum for lower concentrations and minimum for maximal concentrations) is computed and normalised by its final. The variance method described by Brown et al. (2004) is used to calculate mixing times:

$$\log \sigma^2_{RMS} = \log \left\{ \frac{1}{np} \sum_{i=1}^{np} (C_i - 1)^2 \right\} \tag{3}$$

where np is the number of probes and C_i the normalised signal of the probe i. Mixing is considered complete when $\log \sigma^2_{RMS} = -2.6$, corresponding to an average standard deviation of 5% from the final concentration in the column. Mixing times have been measured inside the column for each distributor and for superficial gas velocities ranging between 0.4 and 8 mm/s, which correspond to gas flowrates between 0.1 and 2 m^3/h. Repeated experiences were used to estimate the maximal mixing time error, which is found to be ± 3 s. The error is primarily related to the difficulty to inject the tracer exactly at the same location in the tank for each test, as a small displacement of 1 or 2 mm of the injection device induces an asymmetry on the dye injection. The method has been nevertheless successfully compared to a more classical conductivity method by Gabelle et al. (2011).

3. CFD modelling

2D axisymmetric transient simulations are performed using Fluent Ansys 14.5 CFD code. The choice of 2D simulations is legitimated by the work of Svendsen et al. (1992), who have experimentally observed that both gas and liquid flow patterns in a similar bubble column are axisymmetric and that good agreements between experiments and axisymmetric simulations are often reached. Furthermore, preliminary 3D unsteady simulations have been performed and have converged towards a steady axisymmetric flow. As low gas velocities are involved, simulations converge to stationary flows, which justifies the use of 2D axisymmetric calculations. Simulations are carried out only in the configuration with the first gas distributor. The gas inlet is associated to an effective gas volume fraction $\alpha_G = 0.05$ and with a

velocity that is adjusted to the targeted superficial gas velocity. The distributor with 35 holes is considered as an equivalent porous plate of 28 cm of diameter. Walls are set with a no slip-condition and the top of the column to an atmospheric pressure outlet. The gas layer at the top of the column is simulated in order to separate properly both phases. The gas layer occupies 16% of the total volume of the computational domain. A first order pressure-based solver is used with an implicit unsteady formulation. Gradients are estimated by a Green–Gauss cell based method. Then, momentum, volume fraction, turbulent kinetic energy and specific dissipation rate are solved using a First Order Upwind numerical scheme. Scalar concentration is solved using a Second Order Upwind numerical Scheme. The coupling between pressure and velocity is made with the SIMPLE algorithm. Physical properties used in the simulations are: ρ_L=998 kg/m^3, μ_L=0.001 Pa s, ρ_G=1.20 kg/m^3, μ_G=2.24 · 10^{-5} Pa s. Calculations are considered to be converged when all the normalised residues at each time step fall under 10^{-4} or when a maximum of 50 iterations per time step is achieved, but this latter criterion is effective only during the transitory flow and is not used when the flow is established as residues lower than 10^{-4} are reached. The time step is set to 0.01 s for all cases except for the smallest flow rate (Q=0.1 m^3/h) for which it is set to 0.001 s in order to avoid the solver divergence. The mesh is composed of 0.002 m side squares for a total number of 26250 cells. Sensitivity to the mesh grid spacing has been assessed by comparing the reference mesh with a thinner one based on 0.001 m cells. The relative differences on the maximum liquid velocity, volume average gas holdup and turbulent viscosity are lower than 3%. The injection time of the tracer into the bubble column constitutes less than 10% of the mixing time for small flow rates. As a consequence, it is considered as instantaneous, and during the simulations, the tracer is introduced punctually using a cylindrical patch of 0.05 m height and 0.05 m diameter. The standard deviation of the scalar concentration is used to calculate the mixing time during CFD simulations. This is equivalent to using Eq. (3) with an infinite number of probes.

The numerical simulations are based on the two-fluid model with an Euler–Euler approach. The standard Euler–Euler equations for mass and momentum of phase k are written below:

$$\frac{\partial \alpha_k \rho_k}{\partial t} + \nabla \cdot (\alpha_k \rho_k \mathbf{u}_k) = 0 \tag{4}$$

$$\frac{\partial}{\partial t}(\alpha_k \rho_k \mathbf{u}_k) + \nabla \cdot (\alpha_k \rho_k \mathbf{u}_k \mathbf{u}_k) = -\alpha_k \nabla P + \alpha_k \rho_k \mathbf{g} + \mathbf{F}_{kl} + \nabla \cdot (\alpha_k \boldsymbol{\tau}_k) \tag{5}$$

where $\mathbf{F}_{kl}$ is the interfacial momentum exchange, and $\boldsymbol{\tau}_k$ the stress tensor expressed as:

$$\tau_k = \mu_{eff,k}\left(\nabla \mathbf{u}_k + \nabla \mathbf{u}_k^T - \frac{2}{3} I k\right) \tag{6}$$

The $\mathbf{F}_{kl}$ term corresponds to the interaction forces between the phases. It verifies the interfacial momentum balance $\mathbf{F}_{GI} = -\mathbf{F}_{LI}$. The predominant force to be considered in such system is the drag force (Svendsen et al., 1992; Laborde-Boutet et al., 2009):

$$\mathbf{F}_{GI} = -K_I(\mathbf{u}_G - \mathbf{u}_I) \quad \text{with} \quad K_I = \frac{3\alpha_g \rho_l}{4 d_B} C_D |\mathbf{u}_g - \mathbf{u}_l| \tag{7}$$

Following Hibiki and Ishii (2007), the lift force is negligible for bubbles of 5–6 mm, it is thus neglected, as well as the virtual mass. The choice of the drag coefficient is discussed in Section 4.1. RANS models are commonly used to simulate bubble columns (Jakobsen et al., 2005), and different approaches can be used to model the Reynolds stress tensor of both phases. In the present work, the turbulence k–ω model (Wilcox, 1998) has been used for the stress tensor in the liquid phase as it is preconised in the case of moderate Reynolds number. A standard wall treatment is used. The tensor of the gas phase is modelled following Tchen's (1947) theory. The Bubble Induced Turbulence is not taken into account in the transport equations of k and ω. Preliminary simulations involving the model of Sato et al. (1981) have shown a negligible effect on the liquid velocity profile, on the total turbulent viscosity and on the simulated mixing time which decreases of less than 0.5 s. For this reason the model of Sato has not been considered thereafter.

The transport equation solved for each scalar Φ_j into the liquid phase introduces an effective diffusion coefficient tensor $\boldsymbol{\Gamma}_j$.

$$\frac{\partial \rho_l \Phi_j}{\partial t} + \nabla.(\rho_l \mathbf{u}_l \Phi_j - \boldsymbol{\Gamma}_j \nabla \Phi_j) = 0 \tag{8}$$

In the present work, the effective diffusion coefficient is modelled as the sum of two different contributions: the turbulent diffusion D_t and the bubble-induced diffusion $D_{i,i}$ given in Eq. (2). The molecular diffusivity is neglected into the simulations. The tensor $\boldsymbol{\Gamma}_j$ is diagonal and the two terms (in 2D) are calculated as follows:

$$\Gamma_{j,i} = \rho_l (D_t + D_{i,i}) \tag{9}$$

Implementation of the present model is realized through a routine involving Eqs. (1) and (2). A preliminary validation step has been conducted by simulating the dispersion of scalars in a stagnant flow for different values of the diffusivity coefficients $D_{i,i}$.

4. Results

The results are divided into two parts. Firstly, experimental and simulated hydrodynamics are considered. Second, the transport of scalars is introduced and experimental and numerical mixing times are compared and discussed. The three gas distributors are experimentally investigated but only the first one (#1 with 35 holes) is considered in CFD simulations

4.1. Hydrodynamics

Bubble diameter, terminal velocity and gas holdup are measured during the experiments. Mean Sauter bubble diameter measured during experiments is presented in Fig. 3. For the first gas distributor (35 holes), the bubbles size is almost constant. Consequently, in the simulation, the bubbles diameter is fixed to 5.6 mm and a constant drag coefficient is chosen in order to obtain a bubble terminal velocity of 0.2 m/s, consistent with the experiments. Gas holdups resulting from CFD simulations are compared to experiments in Fig. 4 and a good agreement is found.

As no measurement of the liquid velocity profile has been done, axial velocity profiles resulting from the simulations are compared

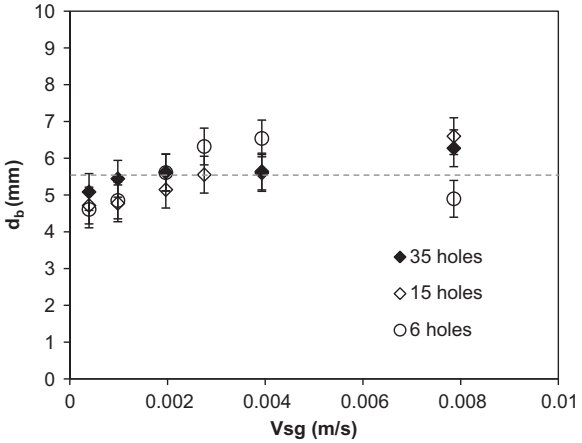

Fig. 3. Bubbles Sauter diameter versus superficial gas velocity (3 distributors).

to correlations proposed by Linneweber (1981), Joshi (1983), Kawase and Moo-Young (1986) or Bernemann (1989). Correlations depend on the liquid velocity at the centre of the column. In Fig. 5, simulated liquid velocity profiles are compared to the calculated ones for Q_g=0.5 m^3/h at a height of 40 cm above the gas injection, when using the liquid velocity at the centre calculated by CFD. Even though there is a scattering at wall, the overall liquid velocity profiles are fairly similar. As discussed earlier, the turbulent viscosity is an important parameter for the scalar transport. Hence the volume averaged turbulent viscosity ν_t is compared to 3 existing correlations (Riquarts, 1981; Denavathan, 1991; Burns and Rice, 1997) for different gas flow rates. Proposed correlations are also more suitable for higher gas velocities, but the comparison can help analysing the global behaviour of the turbulence model. Results are reported in Fig. 6. Correlations are also scattered, but the CFD results are in the range of the correlations. Simulations have also been performed with other turbulence models as $k-\varepsilon$ and RNG $k-\varepsilon$. No significant effects on the gas holdup have been found, but variations of the mean turbulent viscosity of the order of $\pm$15% have been observed. Following Eq. (1), this may lead to proportional variations of the turbulent diffusivities if no additional dispersion phenomenon is considered. Finally, gas holdup calculations are validated, and liquid phase velocity and turbulent viscosity are in agreement with literature. Therefore simulated hydrodynamics are considered satisfactory for the present purpose.

4.2. Mixing times

Experimental mixing times measured with the 3 distributors are reported in Fig. 7. The 3 configurations lead to similar results. A slope as $1/\sqrt{\alpha_g}$ is observed for all the configurations. Lowest mixing times are reached with the largest gas distributor (#1). When mixing is driven by a diffusion D in a vessel of characteristic length L, the mixing time is given by $T_m \propto L^2/D$. A first simplistic

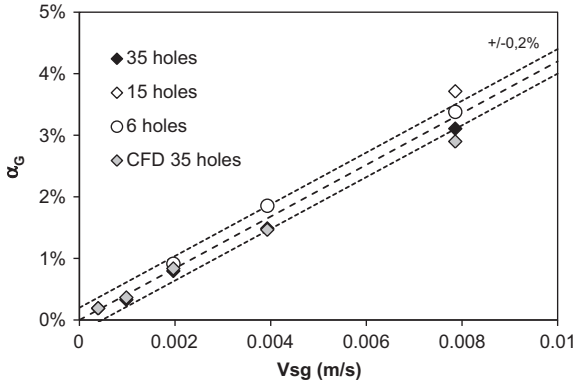

Fig. 4. Gas holdup: experiments (3 distributors) and CFD simulation (distributor 1).

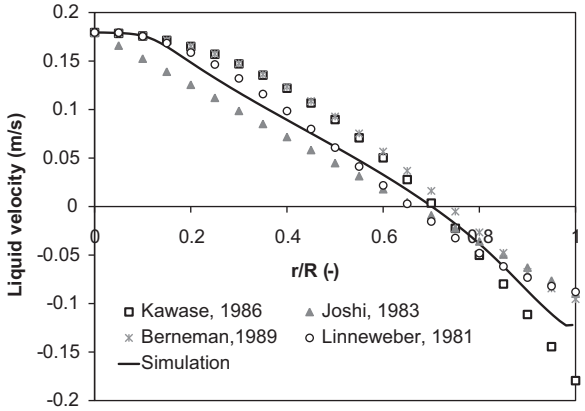

Fig. 5. Liquid velocity profile: CFD and correlations.

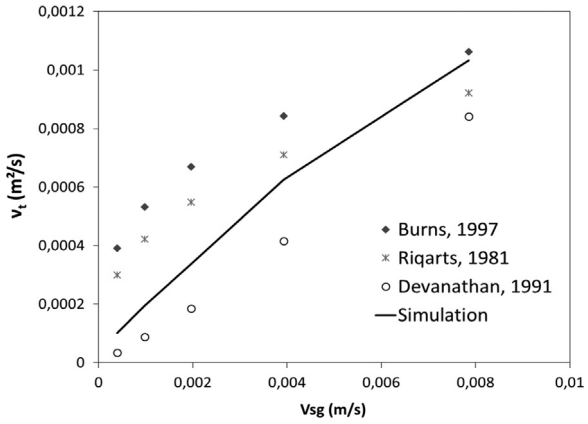

Fig. 6. Volume average turbulent viscosity: CFD and existing correlations versus V_{sg}.

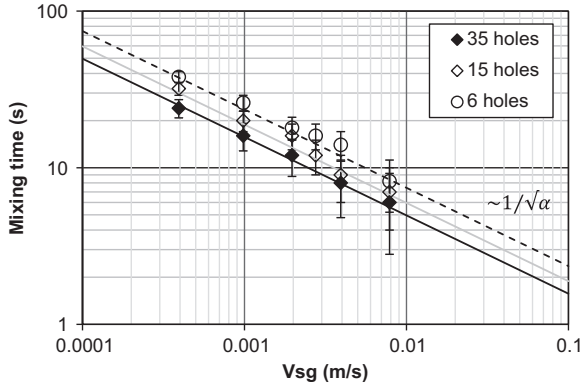

Fig. 7. Experimental mixing times for the 3 distributors. The 3 lines corresponds to $1/\sqrt{\alpha}$ slopes.

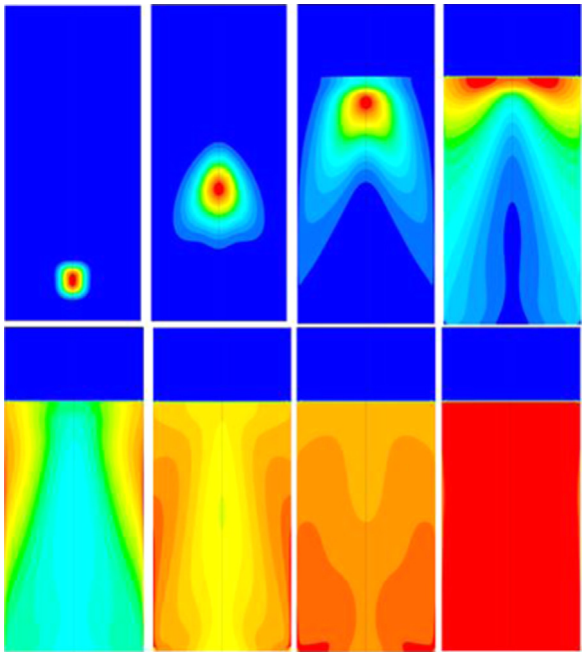

Fig. 8. CFD snapshots of concentration fields during scalar mixing simulation with Sc_t=0.7 including the model of Alméras et al. (2015). Q_g=0.5 m^3/h, t=0, 2, 4, 6, 8, 10, 12, 14 s from left up to right down.

analysis of this result leads to a global apparent diffusivity following $\propto \sqrt{\alpha_g}$ for all flow configurations. This dimensional analysis is coherent with the model of Alméras (Eq. (2)) as only gas volume fractions lower than $\alpha_{gc,i}$ are investigated in the present study. It could indicate that the turbulent contribution to scalar diffusion is moderate.

Concerning CFD simulations of concentration, two models of diffusivity are considered. The first one only involves a turbulent Schmidt number (Eq. (1)) while in the second one the specific contribution of the B.I.T. (Eq. (2)) is added to that of the S.I.T. (Eq. (1)). In both cases, the Sc_t number is swept in the range [0.005–1.5]. Snapshots of the scalar transport simulation are presented in Fig. 8 for Q_g=0.5 m^3/h, with Sc_t=0.7 and including the model of Alméras et al. (2015), at different times (from 0 to 14 s). The snapshots illustrate the transport of the scalar by the liquid recirculation and its dispersion inside the vessel due to the conjugated effect of S.I.T and B.I.T. In Fig. 9, the influence of the Schmidt number on the resulting mixing times is presented for a gas flow rate of Q_g=0.5 m^3/h. Without any other contribution than the turbulent viscosity, the Sc_t number has to be reduced to 0.1 to approach the experimental mixing time. On the other hand, adding the model of diffusivity induced by bubbles leads to common values of the Sc_t number for single-phase turbulence ($\sim$0.7–1) (Combest et al., 2011). These two main observations are still valid for every gas flow rate.

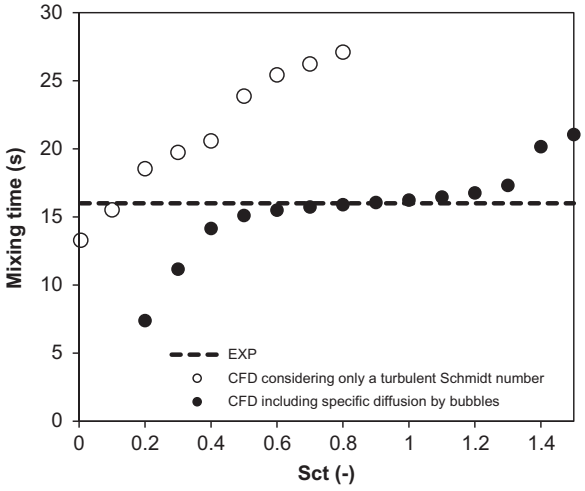

Fig. 9. Mixing time from simulations at Q_g=0.5 m^3/h and for various Sc_t numbers. Including or not the diffusivity model of Alméras et al. (2015).

Fig. 10 presents the simulated mixing time taking into account or not the specific diffusion induced by bubbles (B.I.T.) for every considered gas flow rates and for various values of the Schmidt number. When only the turbulent diffusion is considered (upper part of Fig. 10), the Sc_t number has to be lowered to 0.2 or even 0.1 to obtain mixing times in agreement with experiments. Furthermore the effective Sc_t number strongly depends on the operating conditions. However, considering a Sc_t number of 0.7–1 and adding the diffusivity induced by B.I.T. leads to an evolution of the mixing time in good agreement with the experiments for every gas flow rates without any parameters adjustment (down part of Fig. 10). In this last case, simulated mixing times are poorly sensitive to the Sc_t number, as long as it stays in the range [0.7–1], in agreement with Fig. 9 where a plateau is observed. For $Sc_t > 1.2$, an increase of the mixing time is also observed, which indicates that the S.I.T contribution to diffusivity is not yet negligible. A simple comparison of ν_t reported in Fig. 6 and the contribution of B.I.T from Eq. (2) also lead to the same conclusion.

5. Conclusions

In this work mixing of a passive scalar has been investigated experimentally and numerically in complex bubbly flows at moderate gas holdup ($\alpha_g \leq 3\%$). Experimental mixing times have been measured by an in-house image processing for three gas injection devices. An evolution of the mixing times following $1/\sqrt{\alpha_g}$ trend has been observed. The mixing experiments based on 35 holes for gas injection have been used as validation data for numerical modelling.

For this purpose, the commercial Eulerian RANS model implemented in Fluent has been used and 2D axisymmetric simulations have been performed. Hydrodynamics modelling has been validated first by comparing the simulated global gas volume fraction to experiments. Then, normalised liquid velocity profiles and turbulent viscosities have been compared to correlations. Mixing-time experiments have then been simulated by adding or not the contribution of B.I.T. modelled by Alméras et al. 2015. Various values of the Sc_t number from 0.1 to 1 have been tested too. A good agreement between experiments and modelling is reached with expected values of Sc_t number in the range of [0.7–1] only when the specific diffusivity induced by the bubbles is accounted for. If not, dramatically low values of Sc_t number have to be assigned to approach experimental mixing times.

As a conclusion, the comparison between experiments and CFD modelling shows that the B.I.T. contribution to scalar diffusivity

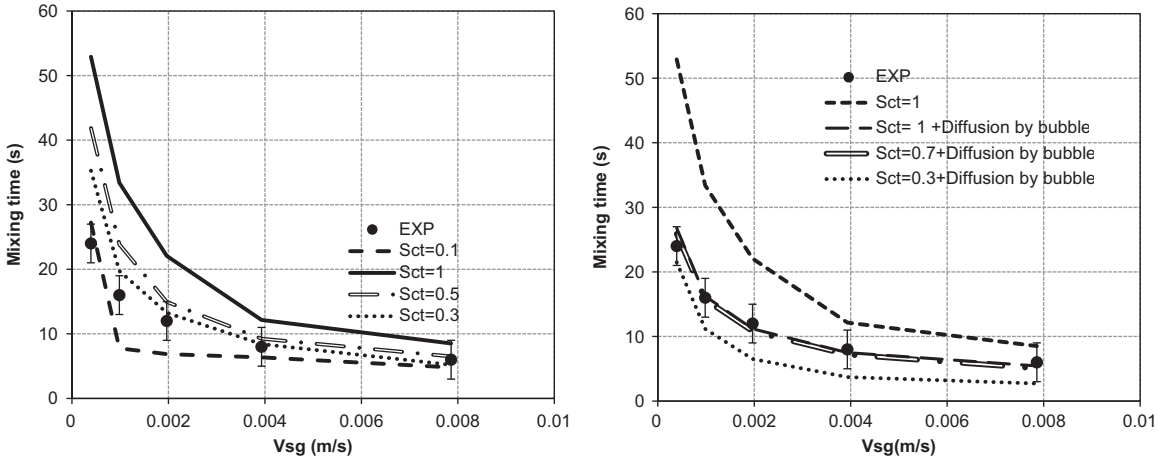

Fig. 10. Mixing time versus V_{sg}. CFD and experimental results. Top: only considering a turbulent Schmidt number. Down: including both a turbulent Schmidt number and the diffusivity model of Alméras et al. (2015).

impacts strongly the mixing in the investigated flows, and has to be taken into account as an explicit contribution independent of the Shear-Induced Turbulence to predict well the mixing of scalars.

Nomenclature

a_i	constant in the calculation of D_{i0}, dimensionless
C_D	Drag law coefficient, dimensionless
C_i	Normalised concentration of tracer at probe I, dimensionless
d, d_B	Bubble diameter (m)
D	Isotropic diffusivity coefficient, $m^2\ s^{-1}$
D_{i0}	Constant in Eq. (2), $m^2\ s^{-1}$
$D_{i,i}$	Diffusion coefficient in direction i accounting for anisotropic diffusion by bubbles, $m^2\ s^{-1}$
D_t	Diffusion coefficient accounting for isotropic diffusion by turbulence, $m^2\ s^{-1}$
$\boldsymbol{F}_{kl}$	Interaction force between gas and liquid, $kg\ m^{-2}\ s^{-2}$
g	Gravity, $m^2\ s^{-1}$
H	Height of the tank, m
i	index for direction (x, y), dimensionless
j	index for scalar, dimensionless
I	Identity matrix, dimensionless
k	Turbulence kinetic energy, $m^2\ s^{-2}$
K_{kl}	Momentum exchange coefficient, $kg\ m^{-1}\ s^{-1}$
L	Characteristic length scale, m
np	Number of probes, dimensionless
P	Pressure (Pa) in Eq. (7), $kg\ m^{-1}\ s^{-2}$
Q, Q_g	Flow rate, $m^3\ h^{-1}$
Sc_t	Turbulent Schmidt number, dimensionless
t	Time, s
T_m	Characteristic time of the transport of scalar, s
$\boldsymbol{u}_k$	Velocity vector of phase k (k=g for gas and k=l for liquid), $m\ s^{-1}$
$\boldsymbol{u}'_k$	Vector of velocity fluctuation of phase k, $m\ s^{-1}$
$\boldsymbol{u}_k^T$	Transposed vector of phase k velocity, $m\ s^{-1}$
$u_i'^2$	Variance of the liquid velocity fluctuation in the direction i, $m^2\ s^{-2}$
U_R	Relative velocity between gas and liquid, $m\ s^{-1}$
V_{sg}	Superficial gas velocity, $m\ s^{-1}$

Greek

$\alpha_{gc,i}$	Volume fraction threshold in direction i, in Eq. (2), dimensionless
α_k	Volume fraction of phase k (k=g for gas and k=l for liquid), dimensionless
α_l	Liquid volume fraction, dimensionless
β	Constant in Eq. (2), dimensionless
ε	Energy dissipation rate, $m^2\ s^{-3}$
Φ_j	Jth scalar, dimensionless
γ_i	Constant for standard deviation of average squared velocity fluctuations, dimensionless
$\Gamma_{j,i}$	Diffusion coefficient on direction I, $m^2\ s^{-1}$
$\boldsymbol{\Gamma_j}$	Diffusion coefficient tensor, $m^2\ s^{-1}$
Λ	Eulerian integral length scale, m.
μ_k	Dynamic viscosity of phase k (k=g for gas and k=l for liquid), $kg\ m^{-1}\ s^{-1}$
$\mu_{eff,k}$	Effective viscosity of phase k (k=g for gas and k=l for liquid), $kg\ m^{-1}\ s^{-1}$
ν_t	Turbulent kinematic viscosity, $m^2\ s^{-1}$
ρ_k	Fluid density (k=g for gas and k=l for liquid), $kg\ m^{-3}$
σ_{RMS}	Standard deviation of tracer normalised concentration, dimensionless
τ_k	Viscous stress tensor, $kg\ m^{-1}\ s^{-2}$
ω	dissipation rate, s^{-1}

Acknowledgements

The authors are grateful to Pierre Loup Buiret and Javier Rey Rueda for their active contributions to the experiments and simulations respectively.

References

Alméras, E., Risso, F., Roig, V., Cazin, S., Plais, C., Augier, F., 2015. Mixing by bubble-induced turbulence. J. Fluid Mech. 776, 458–474.

Alméras, E., 2014. Etude des propriétés de transport et de mélange dans les écoulements à bulles (Ph.D. thesis). Toulouse University, Toulouse.

Ayed, H., Chahed, J., Roig, V., 2007. Hydrodynamics and mass transfer in a turbulent buoyant bubbly shear layer. AIChE J. 53, 2742–2753.

Bernemann, K., 1989. Zur Fluiddynamik und zum Vermischungsverhalten der flüssigen Phase in Blasensäulen mit längsangeströmten Rohrbundeln (Ph.D. thesis). University Dortmund.

Brown, A.R.D., Jones, P., Middleton, C.J., Papadopoulos, G., Arik, E.B., 2004. Experimental methods. In: Paul, L.E., Atiemo-Obeng, A.V., Kresta, M.S. (Eds.), Handbook of Industrial Mixing. John Wiley & Sons, Inc., Hoboken, pp. 145–256.

Burns, L.F., Rice, R.G., 1997. Circulation in bubble columns. AIChE J. 43, 1390–1401.

Combest, D.P., Ramachandran, P.A., Dudukovic, M.P., 2011. On the gradient diffusion hypothesis and passive scalar transport in turbulent flows. Ind. Eng. Chem. Res. 20, 8817–8823.

Corrsin, S., 1963. Estimates of the relation between eulerian and lagrangian scales in large reynolds number turbulence. J. Res. Sci. 20, 115–119.

Dai, J., Sterling, J.D., Nadim, A., 2004. in Computational Methods in Multiphase Flow II. In: Mammoli, A.A., Brebbia, C.A. (Eds.), WIT Press, Southampton, pp. 343–351 [ISBN 1-85312-986-0].

Deckwer, W.D., 1992. Bubble Column Reactors. Wiley, Chichester.

Deen, N., Mudde, R., Kuipers, J., Zehner, P., Kraume, M., 2010. Bubble Columns. Ullmann's Encyclopedia of Industrial Chemistry. Wiley-VCH Verlag GmbH & Co., KGaA.

Delnoij, E., Kuipers, J.A.M.H., van Swaaij, W.P.N., 1997. Computational fluid dynamics applied to gas–liquid contactors. Chem. Eng. Sci. 52, 3623–3638.

Devanathan, N., 1991. Investigation of liquid hydrodynamics in bubble columns via computer automated radioactive particle tracking. D.Sc. thesis. Washington University, St. Louis.

Dhotre, M.T., Niceno, B., Smith, B.L., Simiano, M., 2009. Large-eddy simulation (LES) of the large scale bubble plume. Chem. Eng. Sci. 64, 2692–2704.

Gabelle, J.C., Augier, F., Carvalho, A., Rousset, R., Morchain, J., 2011. Effect of tank size on kLa and mixing time in aerated stirred reactors with non-newtonian fluids. Can. J. Chem. Eng. 89, 1139–1153.

Hibiki, T., Ishii, M., 2007. Lift force in bubbly flow systems. Chem. Eng. Sci. 62, 6457–6474.

Jakobsen, H.A., Lindborg, H., Dorao, C.A., 2005. Modeling of bubble column reactors: progress and limitations. Ind. Eng. Chem. Res. 44, 5107–5151.

Joshi, J.B., 1983. Solid–liquid fluidised beds: some design aspects. Chem. Eng. Res. Des. 61, 143–161.

Kantarci, N., Borak, F., Ulgen, K.O., 2005. Bubble column reactors. Process Biochem. 40 (7), 2263–2283.

Kawase, Y., Moo-Young, M., 1986. Liquid phase mixing in bubble columns with newtonian and non-newtonian fluids. Chem. Eng. Sci. 41, 1969–1977.

Laborde-Boutet, C., Larachi, F., Dromard, N., Delsart, O., Schweich, D., 2009. CFD simulation of bubble column flows: investigations on turbulence models in RANS approach. Chem. Eng. Sci. 64, 4399–4413.

Lance, M., Bataille, J., 1991. Turbulence in the liquid phase of a uniform bubbly air–water flow. J. Fluid Mech. 222, 95–118.

Lance, M., Tran, M.L., Petersen, K., 1996. Modelling of gas–liquid flow in bubble regime, oil and gas science and technoloiges. Rev. l'Institut Fr. Pét. 51, 279–289.

Lau, Y.M., Bai, W., Deen, N.G., Kuipers, J.A.M.H., 2014. Numerical study of bubble break-up in bubbly flows using a deterministic Euler–Lagrange framework. Chem. Eng. Sci. 108, 9–22.

Laurent, A., Charpentier, J.C., 1974. Aires interfaciales et coefficients de transfert de matière dans les divers types d'absorbeurs et de réacteurs gaz–liquide. Chem. Eng. J. 8, 85–101.

Li, Y., Zhang, J.P., Fan, L.S., 2000. Discrete-phase simulation of single bubble rise behavior at elevated pressures in a bubble column. Chem. Eng. Sci. 55, 4597–4609.

Linneweber, K.W., 1981. Örtliche Gehalte an Gas sowie an Gas und Feststoff in Blasensäulen (Ph.D. thesis). TU, München.

Politano, M.S., Carrica, P.M., Converti, J., 2003. A model for turbulent polydisperse two-phase flow in vertical channels. Int. J. Multiph. Flow 29, 1153–1182.

Radl, S., Khinast, J.G., 2010. Multiphase flow and mixing in dilute bubble swarms. AIChE J. 56, 2421–2445.
Rafique, M., Chen, P., Dudukovic, M.P., 2004. Computational modeling of gas–liquid flow in bubble columns. Rev. Chem. Eng. 20, 225–375.
Riboux, G., Risso, F., Legendre, D., 2010. Experimental characterization of the agitation generated by bubbles rising at high reynolds number. J. Fluid Mech. 643, 509–539.
Riquarts, H.P., 1981. A physical model for axial mixing of the liquid phase for heterogeneous flow regime in bubble columns. Ger. Chem. Eng. 4, 18–23.
Rzehak, R., Krepper, E., 2013. CFD modeling of bubble-induced turbulence. Int. J. Multiph. Flow 55, 138–155.
Sato, Y., Sadatomi, M., Sekogushi, K., 1981. Momentum and heat transfer in two-phase bubble flow-I. Int. J. Multiph. Flows 7, 167–177.
Serizawa, A., Kataoka, I., Michiyoshi, I., 1992. Phase distribution in bubbly flow. In: Hewitt, G.F., Delhaye, J.M., Zuber, N. (Eds.), Multiphase Science and Technology, 6. Hemishpere Publishing Corporation, Washington DC, pp. 257–301.
Svendsen, H., Jakobsen, H., Torvik, R., 1992. Local flow structures in internal loop and bubble column reactors. Chem. Eng. J. 47, 3297–3304.
Taylor, G.I., 1921. Diffusion by continuous movements. Proc. Lond. Math. Soc. 2–20 (1), 196–212.
Tchen, C.M., 1947. Mean Value and Correlation Problems Connected with the Motion of Small Particles in a Turbulent Fluid (Ph.D. thesis). University of Delft, The Hague.
Troshko, A.A., Hassan, Y.A., 2001. A two-equation turbulence model of turbulent bubbly flows. Int. J. Multiph. Flow 27, 1965–2000.
Wilcox, D.C., 1998. Turbulence Modeling for CFD. DCW Industries, Inc., La Canada, California.
Zhang, D.Z., Prosperetti, A., 1994. Ensemble phase-averaged equations for bubbly flows. Phys. Fluids 6, 2956–2970.